2018

Extracellular superoxide dismutase (SOD3) regulates oxidative stress at the vitreoretinal interface

Katherine J. Wert
Stanford University

Gabriel Velez
Stanford University

Madeline R. Cross
University of Iowa

Brett A. Wagner
University of Iowa

Melissa L. Teoh-Fitzgerald
UNMC, m.teohfitzgerald@unmc.edu

See next page for additional authors

Authors
Katherine J. Wert, Gabriel Velez, Madeline R. Cross, Brett A. Wagner, Melissa L. Teoh-Fitzgerald, Garry R. Buettner, J. Jason McAnany, Alicia Olivier, Stephen H. Tsang, Matthew M. Harper, Frederick E. Domann, Alexander G. Bassuk, and Vinit B. Mahajan

Free Radical Biology and Medicine 124 (2018) 408–419

Contents lists available at ScienceDirect

Free Radical Biology and Medicine

journal homepage: www.elsevier.com/locate/freeradbiomed

Extracellular superoxide dismutase (SOD3) regulates oxidative stress at the vitreoretinal interface☆

Katherine J. Wert[a,b], Gabriel Velez[a,b], Madeline R. Cross[c], Brett A. Wagner[d], Melissa L. Teoh-Fitzgerald[e], Garry R. Buettner[d], J. Jason McAnany[f], Alicia Olivier[g], Stephen H. Tsang[h,i,j], Matthew M. Harper[k,l,m], Frederick E. Domann[d], Alexander G. Bassuk[c], Vinit B. Mahajan[a,b,n,*]

[a] Byers Eye Institute, Department of Ophthalmology, Stanford University, Palo Alto, CA, United States
[b] Omics Laboratory, Stanford University, Palo Alto, CA, United States
[c] Department of Pediatrics, University of Iowa, Iowa City, IA, United States
[d] Department of Radiation Oncology, Carver College of Medicine, University of Iowa, Iowa City, IA, United States
[e] Department of Biochemistry and Molecular Biology, University of Nebraska Medical Center, Omaha, NE, United States
[f] Department of Ophthalmology, University of Illinois at Chicago, Chicago, IL, United States
[g] Division of Comparative Pathology, Department of Pathology, Carver College of Medicine, University of Iowa, Iowa City, IA, United States
[h] Bernard and Shirlee Brown Glaucoma Laboratory and Barbara & Donald Jonas Laboratory of Regenerative Medicine, Columbia University, New York, NY, United States
[i] Edward S. Harkness Eye Institute, Columbia University, New York, NY, United States
[j] Departments of Ophthalmology, Pathology & Cell Biology, and Institute of Human Nutrition, Columbia University, New York, NY, United States
[k] Department of Ophthalmology and Visual Sciences, University of Iowa, Iowa City, IA, United States
[l] Department of Veterans Affairs Iowa City Health Care System, Iowa City, IA, United States
[m] Veterans Affairs Center for the Prevention and Treatment of Visual Loss, Iowa City, IA, United States
[n] Palo Alto Veterans Administration, Palo Alto, CA, United States

ARTICLE INFO

Keywords:
Knockout mouse
Diabetic retinopathy
Vitreous substructures
Antioxidant
Metabolic dysregulation
Proteomics
Extracellular matrix
Vitreous base
Vitreous cortex

ABSTRACT

Oxidative stress is a pathogenic feature in vitreoretinal disease. However, the ability of the inner retina to manage metabolic waste and oxidative stress is unknown. Proteomic analysis of antioxidants in the human vitreous, the extracellular matrix opposing the inner retina, identified superoxide dismutase-3 (SOD3) that localized to a unique matrix structure in the vitreous base and cortex. To determine the role of SOD3, *Sod3*$^{-/-}$ mice underwent histological and clinical phenotyping. Although the eyes were structurally normal, at the vitreoretinal interface *Sod3*$^{-/-}$ mice demonstrated higher levels of 3-nitrotyrosine, a key marker of oxidative stress. Pattern electroretinography also showed physiological signaling abnormalities within the inner retina. Vitreous biopsies and epiretinal membranes collected from patients with diabetic vitreoretinopathy (DVR) and a mouse model of DVR showed significantly higher levels of nitrates and/or 3-nitrotyrosine oxidative stress biomarkers suggestive of SOD3 dysfunction. This study analyzes the molecular pathways that regulate oxidative stress in human vitreous substructures. The absence or dysregulation of the SOD3 antioxidant at the vitreous base and cortex results in increased oxidative stress and tissue damage to the inner retina, which may underlie DVR pathogenesis and other vitreoretinal diseases.

1. Introduction

Reactive oxygen species (ROS) are a consequence of aerobic respiration and substrate oxidation within the cell. At physiological levels, ROS are required for many cellular functions, including immune function and signal transduction [1]. However, excess production or inadequate removal results in oxidative stress through high levels of ROS which can react with macromolecules. Oxidative stress has been implicated in a wide variety of human diseases such as atherosclerosis, hypertension, heart failure, and diabetes [2].

The eye has particularly high levels of oxidative stress for several reasons. First, the retina is the most metabolically active tissue in the human body [3]. Second, the metabolic exchange between the vitreous and systemic circulation is slow [4], which means that the retina must

☆ The authors have no commercial or financial interests associated with this article.

* Corresponding author at: Byers Eye Institute, Department of Ophthalmology, Stanford University, Palo Alto, CA 94304, United States.
E-mail address: vinit.mahajan@stanford.edu (V.B. Mahajan).

https://doi.org/10.1016/j.freeradbiomed.2018.06.024
Received 16 April 2018; Accepted 21 June 2018
Available online 22 June 2018
0891-5849/

cope with a large amount of oxidative stress as a result of the high metabolic activity, yet it has a relatively inefficient exchange process. The retinal pigment epithelium (RPE) and choroid (a large vascular plexus) line the outer retina to remove metabolic waste, but no similar cellular or vascular system exists for the inner retina, since light must reach the retina without interference. Instead, the inner retina is opposed by the vitreous, an optically transparent, extracellular matrix (ECM). How the inner retina manages metabolic waste is not known, but it may be especially vulnerable in metabolic disorders such as diabetes, where intracellular mechanisms are dysfunctional.

Indeed, elevation of intraocular ROS in the vitreous is implicated in the pathogenesis of diabetic vitreoretinopathy (DVR), but the molecular mechanisms are not known. Since oxidative stress is closely linked to the intraocular neovascularization [5,6], inflammation [7], fibrosis, and tractional retinal detachment that characterize DVR, we sought to study the molecular mechanisms of oxidative stress regulation in the vitreous. SODs are a family of enzymes that catalyze the dismutation of superoxide, converting it into hydrogen peroxide and dioxygen. There are several isoforms of superoxide dismutase: SOD1 (cytosolic), SOD2 (mitochondrial), and SOD3 (extracellular) [8]. Mutations within both SOD1 and SOD2 are implicated in human disease, such as amyotrophic lateral sclerosis (ALS) and ischemic heart disease, respectively [9–12]. SOD3 is a secretory, homotetrameric, Cu/Zn-containing SOD that is found primarily in the ECM and on cell surfaces. SOD3 binds heparan sulfate proteoglycans (HSPGs) and collagen which function to anchor it to the ECM. It is hypothesized that these ECM proteins keep SOD3 locally sequestered until needed, and it has been previously shown that the single nucleotide polymorphism (SNP) R213G in SOD3 alters its biodistribution to be in favor of the unbound form [13,14]. Regions of the eye that are composed of higher concentrations of collagen and HSPGs include the vitreous base and the posterior hyaloid. In our study, we found that SOD3 is differentially localized to vitreous substructures through specific proteoglycan interactions to prevent oxidative damage to the adjacent neural retina. Our study shows that dysregulation of SOD3 interactions and activity at the vitreous base may be critical in the pathophysiology of DVR and other oxidative stress-related vitreoretinopathies.

2. Results

2.1. Oxidative stress proteins in the human vitreous

To identify proteins that regulate oxidative stress in the retina and vitreous, we interrogated human proteomics datasets [15] using gene ontology (GO) analysis [16]. There were 75 proteins in the human retina and vitreous categorized as oxidoreductases (Fig. 1A). Of these, there were 6 proteins identified in the retina with known antioxidant activity (GO: 0016209) and 9 in the vitreous. Three antioxidant proteins were unique to the vitreous: superoxide dismutase-3 (SOD3), eosinophil peroxidase (EPX), and arachidonate 5-lipoxygenase-activating protein (ALOX5AP; Fig. 1B) [15]. A network of these interacting proteins was generated (Fig. 1C) [17,18]. Since the vitreous is an ECM and SOD3 was absent from the retina, we hypothesized that extracellular SOD3 may regulate the oxidative stress response in the vitreous. Network analysis of vitreous proteins identified 23 SOD3 interactors, further suggesting that SOD3 may play a role in regulating the oxidative stress response in the vitreous (Fig. 1D).

2.2. SOD3 is concentrated within the vitreous base in a unique and highly organized pattern

To determine if SOD3 was differentially active in the vitreous substructures, the vitreous base, core, and cortex were dissected and analyzed with a xanthine oxidase (XO) based SOD activity assay (Fig. 2A). XO is an enzyme that generates superoxide, and the percent SOD activity of each tissue sample corresponds to the amount of superoxide dismutated. This assay recognizes zinc-bound forms of SOD (SOD1 and SOD3) but not the manganese bound form (SOD2). The level of SOD activity was variable between human eye samples, but activity of SOD was found to be higher within the vitreous base, suggesting that SOD3 may be sequestered at the vitreous base to regulate oxidative stress within the eye (Fig. 2A). To verify SOD3-specific expression in the vitreous substructures of the human eye, and more closely examine the vitreous ECM substructures, we performed immunohistochemistry (IHC) on sagittal sections of human eye vitreous [15]. We found that SOD3 expression was concentrated in the vitreous base (overlying the ciliary body; Fig. S1A-C; Fig. 2B) and vitreous cortex (at the vitreoretinal interface; Fig. S1D-F; Fig. 2C). At higher magnification, SOD3 expression was organized in a looped pattern, reminiscent of the highly organized structures of the ECM in the vitreous (Fig. S1C, F; Fig. 2B, C).

2.3. SOD3 interacts with extracellular matrix proteins in the vitreous

The distinct looped pattern of SOD3 in the vitreous base and cortex suggested that it was binding specific ECM proteins. In order to determine if any of the vitreous collagens or proteoglycans co-localize with the SOD3 expression pattern, several of the ECM proteins that were identified in our vitreous proteomics profiling screen (e.g. decorin and aggrecan; Fig. 1D) were blotted onto PVDF membranes (Fig. 2D). Additional known binding partners for SOD3, such as heparan sulfate proteoglycans (HSPGs) and syndecans 1 and 2 (Syn1 and Syn2), were also blotted on the PVDF membrane. Membranes were incubated with SOD3 protein (left blot, depicted in left cartoon panel), and SOD3 was shown to bind strongly to heparin in the vitreous (Fig. 2D; left blot). Since the c-terminus of SOD3 contains amino acids implicated in interactions with other proteins, we tested recombinant SOD3 missing the heparin-binding domain (HBD; ECSODΔHBD; middle panel) or mutated with R213G in the HBD (right panel) for their ability to interact with purified vitreous proteins and proteoglycans. In non-ocular tissues, both of these mutants fail to interact with their glycosaminoglycan target. In our assay, both the HBD and R213G mutant SOD3 proteins removed the binding signal to heparin in the dot blot assay (Fig. 2D; middle and right blots).

Since both ECM proteins found in our vitreous proteomics screen (decorin and aggrecan) did not seem to bind SOD3 at detectable levels, we confirmed this potential lack of binding for decorin using immunohistochemistry (IHC). We tested SOD3 activity and co-localization in the vitreous base for both heparin (a known binding partner with strong binding on the dot blot assay) and decorin. SOD3 activity was completely blocked in the presence of heparin (data not shown). Both SOD3 (green; open circle) and decorin (red; arrow) localized to the same organized looped pattern within the vitreous base, but no co-localization of SOD3 and decorin was detectable with IHC (Fig. 2E). There may be limited SOD3 co-localization with decorin in the vitreous base that we were unable to detect, but this result suggests that SOD3 interaction with decorin is not the primary interaction responsible for SOD3 sequestration to the vitreous base, and SOD3 binding to heparin is an interaction that occurs within the vitreous base of the human eye. Similar results were found at the vitreous cortex (data not shown).

2.4. Sod3 functions within the mouse vitreous

We have previously published the identification of the vitreous substructures in mice based on anatomical location [19]. It has not been possible to dissect the specific substructures of the mouse vitreous, but IHC of the whole mouse vitreous showed the presence of Sod3 (green; Fig. 3A) concentrated at the vitreous base (labeled vb) and vitreous cortex (labeled vc), similar to the human vitreous SOD3 sequestration. Currently, no data has been published to analyze the *Sod3* knockout phenotype within the eye. Histologically, *Sod3*$^{-/-}$ mice displayed a normal retina, with no signs of cataract or membranes (data not shown). As expected, the *Sod3*$^{-/-}$ mice showed no Sod activity in

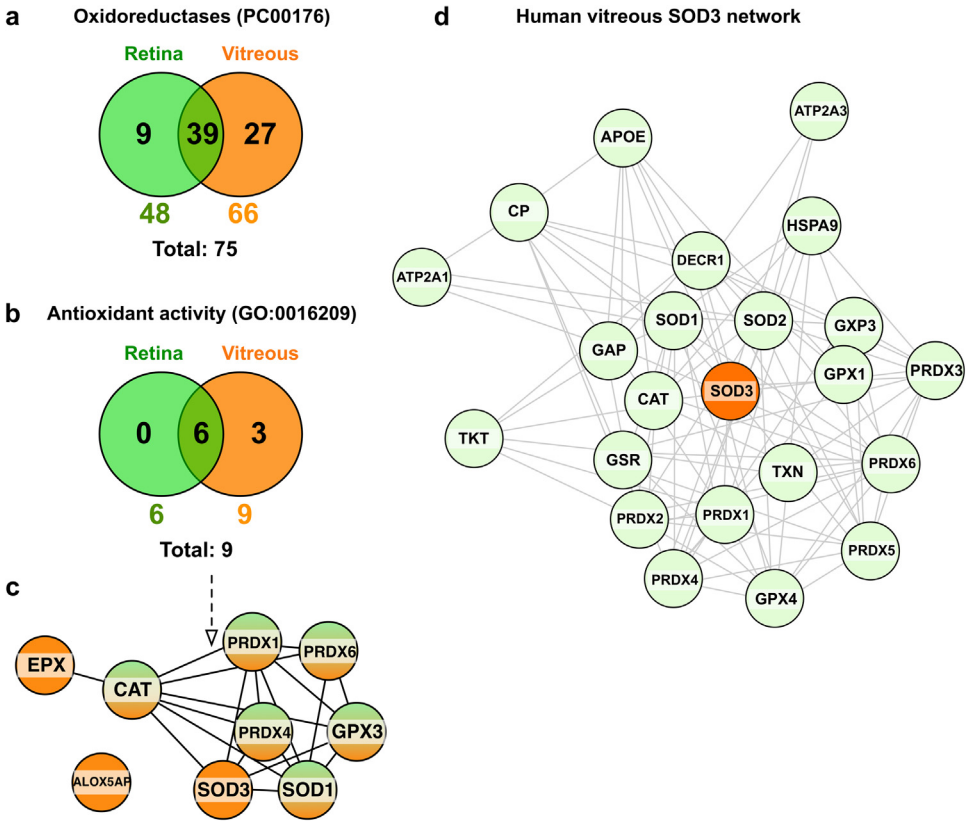

Fig. 1. Interrogation of human retina and vitreous proteomes reveals superoxide dismutase 3 (SOD3) to be present in the vitreous. (A) Gene ontology (GO) analysis was performed on our previously-published human retina and vitreous proteomic datasets. Proteins categorized as oxidoreductases were identified in both tissues. (B) Proteins containing 'antioxidant activity' (GO:0016209) were identified in both tissues. Three of these proteins were unique to the vitreous: superoxide dismutase (SOD3), eosinophil peroxidase (EPX), and arachidonate 5-lipoxygenase-activating protein (ALOX5AP). (C) A network of these antioxidant proteins was generated using STRING and visualized using Cytoscape. Circles represent proteins (nodes) and lines represent known interactions (edges). (D) Network analysis of the 5211 total proteins in the human vitreous identified 23 SOD3 interactors. ATP2A1, Sarcoplasmic/Endoplasmic Reticulum Calcium ATPase 1; ATP2A3, Sarcoplasmic/Endoplasmic Reticulum Calcium ATPase 3; APOE, Apolipoprotein E; CAT, Catalase; CP, Ceruloplasmin; DECR1, Decorin; GAP, GTPase Activating Protein; GPX1, Glutathione Peroxidase 1; GPX3, Glutathione Peroxidase 3; GPX4, Glutathione Peroxidase 4; GSR, Glutathione Reductase, Mitochondrial; HSPA9, Stress-70 Protein, Mitochondrial; PRDX1–6, Peroxiredoxin 1–6; SOD1, Superoxide Dismutase 1; SOD2, Superoxide Dismutase 2; TKT, Transketolase; TXN, Thioredoxin.

comparison to their wild-type controls (Fig. 3B).

2.5. Loss of Sod3 leads to increased oxidative stress at the vitreoretinal interface

Since SOD3 is an important regulator of oxidative stress, potential oxidative stress markers related to the loss of Sod3 function were studied within the mouse vitreous and inner retina. Nitrates and 3-nitrotyrosine are byproducts of oxidative stress, and elevated levels of nitrate or 3-nitrotyrosine indicates increased oxidative stress. Sievers nitrate analysis showed no change in nitrate levels between *Sod3*$^{-/-}$ mice and control mice (Fig. 3C). However, 3-nitrotryosine was elevated in both the vitreous and the retinal ganglion cell (RGC) layer of the *Sod3*$^{-/-}$ mice in comparison to controls (Fig. 3D). 3-nitrotyrosine expression was comparable between both the *Sod3*$^{-/-}$ mice and controls in the outer retinal layers, suggesting that Sod3 plays a key role in oxidative stress regulation at the vitreoretinal interface.

2.6. Loss of Sod3 causes inner retinal dysfunction

Since the ocular phenotype of *Sod3*$^{-/-}$ mice has not been characterized, we analyzed these mice for clinical pathologies that may be found in human patients with ocular disorders related to increased oxidative stress. Optical coherence tomography (OCT) was used to determine whether there was a loss of the neural retinal layers. Five recordings were taken of the neural retina thickness at the same scan line of the eye, at both the scleral (OCT-S) and optic nerve head regions (OCT-ONH). No significant changes were found in the thickness of the neural retina between *Sod3*$^{-/-}$ mice and their controls (Fig. 4**A**). Intra-ocular pressure was then recorded from male mice at 4 months of age, with 4 recordings per eye, with no significant difference ($p = 0.4$; Fig. 4**B**). To further examine the RGCs, where increased 3-nitrotyrosine was found at the vitreoretinal interface (Fig. 3D), we performed pattern electroretinograms (PERGs), which reflect inner retinal electrophysiology, on the *Sod3* knockout mice and their controls (Fig. 4C). Representative traces displayed a loss of function from the RGCs in the *Sod3*$^{-/-}$ mice (blue trace) compared to controls (black trace; Fig. 4C; top panel). Quantification of the cohort of mice analyzed showed a loss of RGC function in the *Sod3*$^{-/-}$ mice based on a significantly reduced P50 to N95 PERG amplitude ($p = 0.0054$; Fig. 4C; middle). N95 latency times were trending lower in the *Sod3*$^{-/-}$ mice compared to controls; however, these were not significantly changed between groups ($p = 0.22$; Fig. 4C; lower). Full-field ERGs, which reflect whole retinal electrophysiology, were normal (data not shown), indicating the physiological defect localized to the inner retina and not the outer retina. Thus, the loss of Sod3 leads to a significant decline in PERG inner retinal responses, a clinical phenotype seen in human patients with diabetic vitreoretinopathy (DVR) and other vitreoretinopathies. This finding was also consistent with the increased oxidative stress observed at the inner retina of *Sod3*$^{-/-}$ mice.

We then treated the *Sod3*$^{-/-}$ mice with Tempol (4-hydroxy-2,2,6,6-tetramethylpiperidine-*N*-oxyl). Tempol is a redox-cycling nitroxide water-soluble SOD mimetic agent that acts as a potent antioxidant by reducing oxidative stress from the metabolism of a large variety of cellular reactive oxygen and nitrogen species [20–23]. To provide Tempol for the long-term duration of the experiment, *Sod3*$^{-/-}$ mice and respective controls were placed on Tempol via their drinking water. To offset the taste of Tempol and ensure that the mice drink their water for a steady dosage, sucrose was added into the drinking water. An additional experimental group for both wild-type and *Sod3*$^{-/-}$ mice were placed on sucrose-only drinking water during the duration of the experiment. Representative traces for each of the four experimental groups are shown in Fig. 5A, as compared to representative control traces shown in Fig. 4C. We then quantified the PERG responses for all groups, both controls and experimental mice (Fig. 5B). Unexpectedly, the addition of sucrose alone to the drinking water caused for a

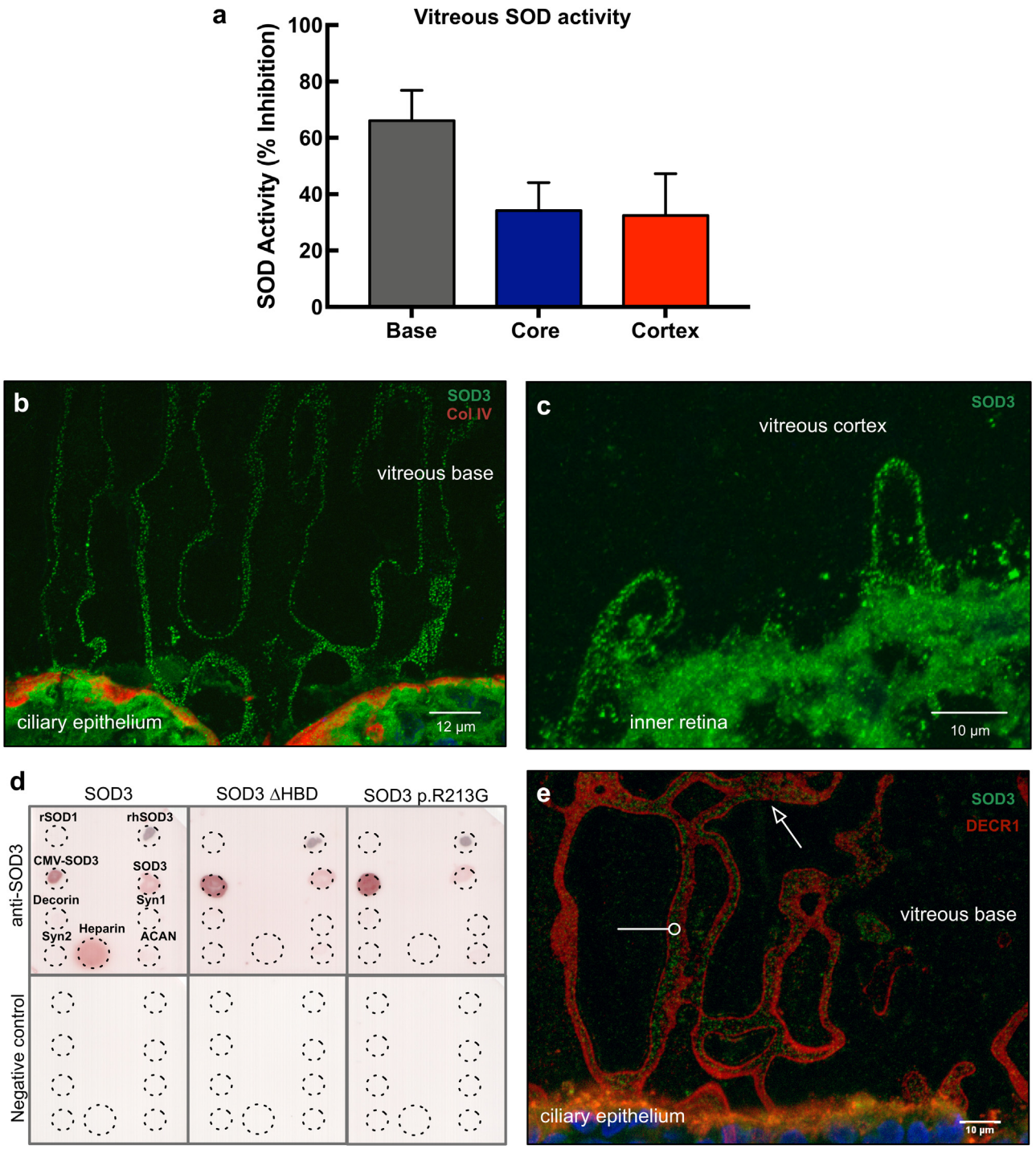

Fig. 2. SOD3 is concentrated in the human vitreous base and cortex in a highly organized, looped pattern. (A) Specific vitreous substructures (base, core and cortex) were dissected and SOD activity (from both SOD1 and SOD3) was determined using a xanthine oxidase assay. Error bars = SEM. N = 3 replicates per sample and 4 vitreous samples per substructure. (B) IHC for SOD3 (green) shows a unique looped pattern located within the vitreous base. Collagen IV (red) stains the basal lamina. Scale bar, 12 µm. (C) IHC for SOD3 (green) shows a unique looped pattern located within the vitreous cortex, by the vitreoretinal interface. Scale bar, 10 µm. (D) Human SOD3 (SOD3; left cartoon panel), human recombinant SOD3 with a deletion of the heparin/collagen binding domain (SOD3ΔHBD; middle cartoon panel), and human recombinant SOD3 with the R213G mutation in the heparin/collagen binding domain (SOD3 R213G; right cartoon panel) were incubated on a PVDF membrane in a dot blot assay against glycosaminoglycans (GAGs) and extracellular matrix (ECM) proteins found in the vitreous (top blots). Negative control blots without SOD3 incubation are shown below. rSOD1, recombinant superoxide dismutase 1; rhSOD3, recombinant human superoxide dismutase 3; CMV-SOD3, superoxide dismutase 3 purified after over-expression with the cytomegalovirus ubiquitous promoter in human cells; SOD3, purified superoxide dismutase 3; Syn1, syndecan 1;Syn2, syndecan 2; ACAN, aggrecan. (E) Immunostaining confirmed that decorin (red; arrow) was present in the looped pattern in the human vitreous base but did not co-localize with SOD3 (green; white circle). Cell nuclei were stained by DAPI (blue). Scale bar, 10 µm.

significant increase in inner retinal function in the *Sod3*$^{-/-}$ mice (orange) compared to untreated *Sod3*$^{-/-}$ mice (p = 0.0141; blue), but not in the wild-type mice (p = 0.3698; black and gray; Fig. 5B). However, the addition of Tempol to the drinking water enhanced the inner retinal function in both the wild-type (p = 0.0353; green; Fig. 5) and *Sod3*$^{-/-}$ mice (p = 0.0151; red; Fig. 5). However, there was no significant

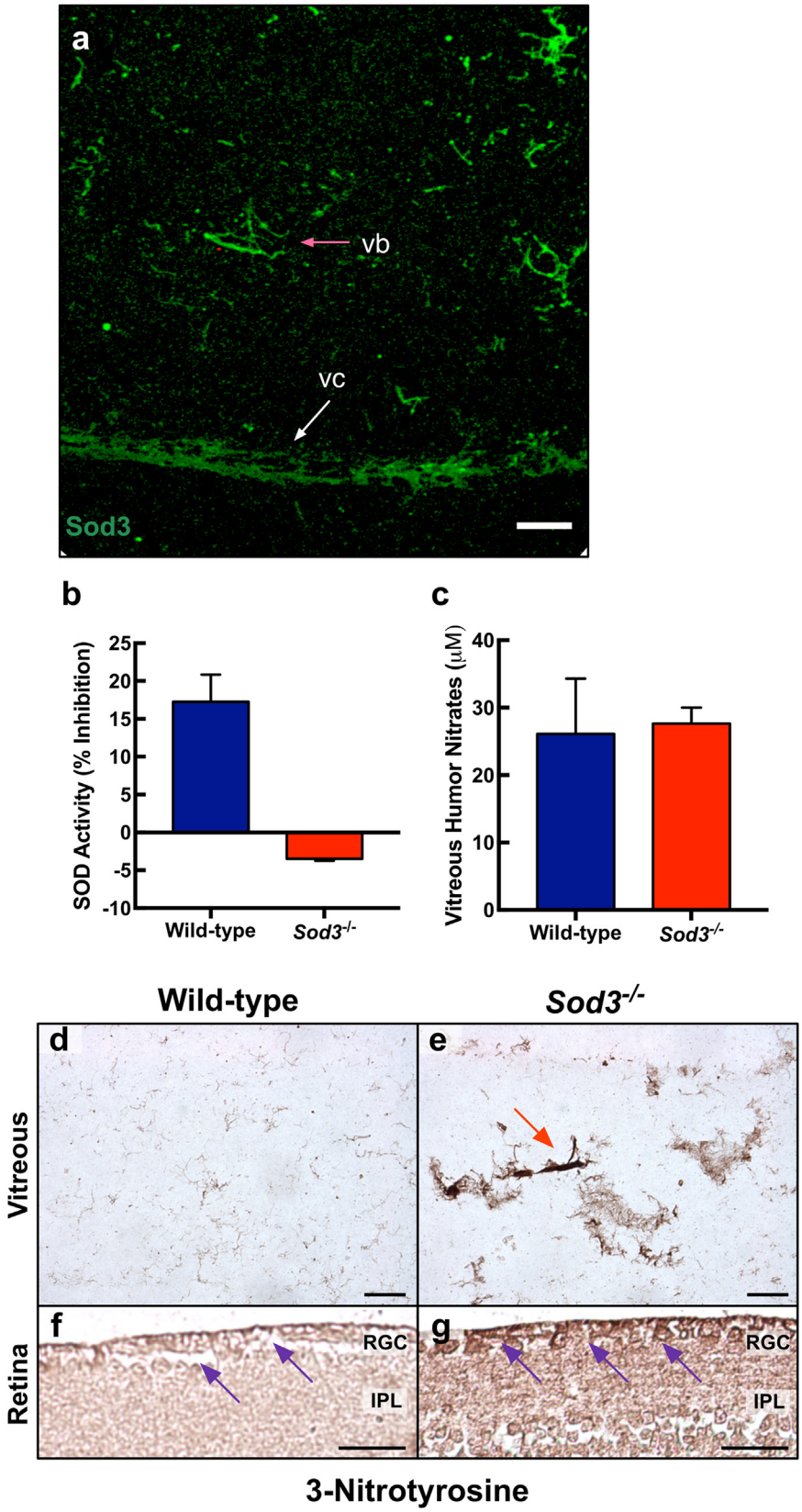

Fig. 3. Sod3 is detectable in the vitreous base and cortex of the mouse eye and loss of Sod3 results in increased oxidative stress. (A) IHC confirmed the presence of Sod3 (green) within the mouse vitreous base (red arrow) and concentrated at the vitreous cortex (white arrow). Scale bar = 20 μm. VB, vitreous base; VC, vitreous cortex. (B) Sod3 knockout mice had no Sod3 activity compared to wild-type controls, based on a xanthine oxidase assay ($p = 0.0045$). N = 3 replicates per group. (C) Nitrate levels in the mouse vitreous remained unchanged between wild-type and Sod3 knockout mice. N = 5 replicates per mouse, 2 mice analyzed per group. Error bars represent the standard error of the mean. (D-E) IHC showed that 3-nitrotyrosine was increased within the Sod3 knockout mouse vitreous (red arrow) compared to a wild-type mouse. (F-G) 3-Nitrotyrosine was also increased within the retinal ganglion cell layer of the neural retina and at the vitreoretinal interface (purple arrows).

difference between mice treated with sucrose alone compared to mice treated with Tempol and sucrose ($p = 0.9566$ for wild-type mice and $p = 0.9961$ for *Sod3*$^{-/-}$ mice). Overall, both sucrose and sucrose with Tempol delivered via the drinking water was able to offset the loss of inner retina function detectable by PERG in mice lacking Sod3.

2.7. Human diabetic vitreoretinopathy

Oxidative stress is a key feature of human DVR [24]. Compared to a normal human fundus (Fig. 6A), patients with early stages of DVR exhibit a loss of inner retinal function, visible using PERG (Fig. 6B). The

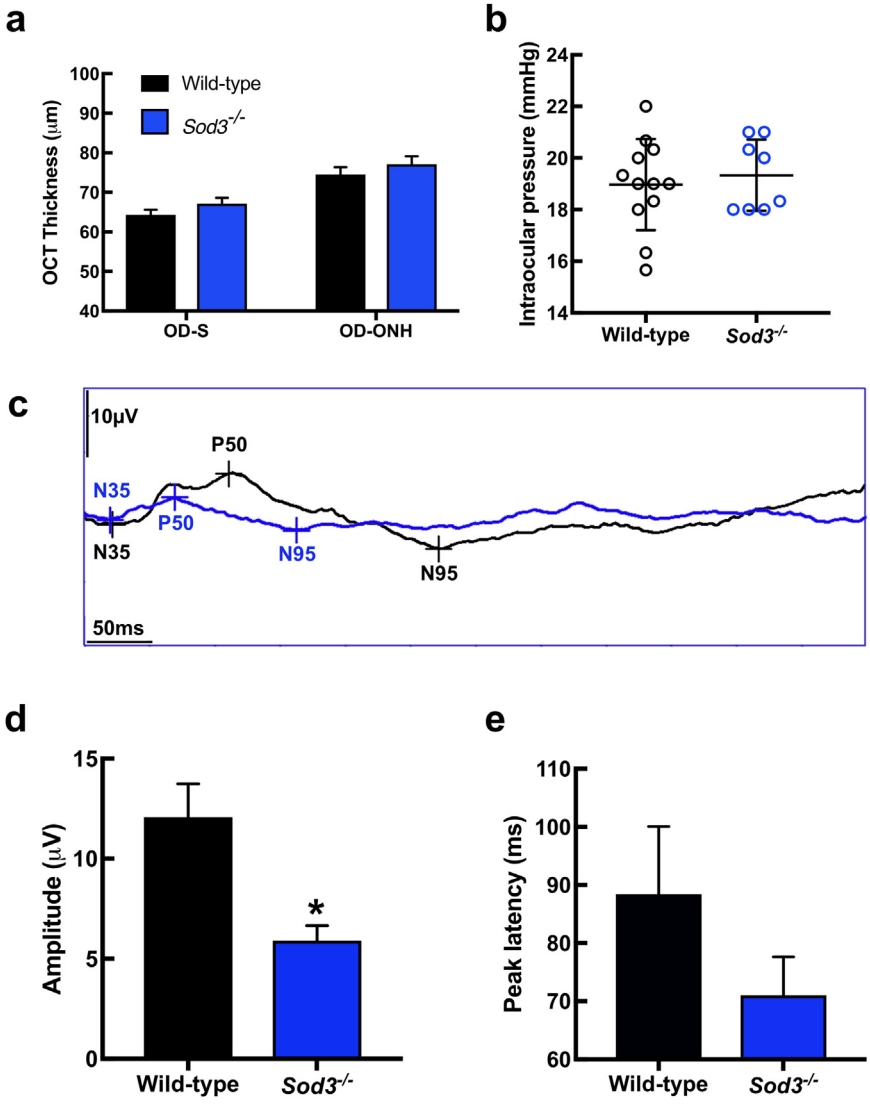

Fig. 4. Loss of Sod3 leads to inner retinal dysfunction. (A) Thickness of the neural retina was determined using optical coherence tomography (OCT) at both the scleral (OCT-S) and optic nerve head (OCT-ONH) regions of the retina. All recordings were taken from the same scan line (19/32) and 5 recordings per eye were used for analysis. N = 6 *Sod3*$^{+/+}$ mice and 7 *Sod3*$^{-/-}$ mice. (B) Intraocular pressure was found to trend slightly higher in the Sod3 knockout mice compared to wild-type controls, although not significantly altered ($p = 0.4$). All mice examined were males at 4 months of age, with 4 recordings per eye. N = 6 mice for *Sod3*$^{+/+}$ and 4 mice for *Sod3*$^{-/-}$. (C) Representative traces from the pattern electroretinogram (pERG) showed a decline in visual response in the *Sod3*$^{-/-}$ mouse (blue) compared to a *Sod3*$^{+/+}$ control mouse (black; top). Quantification of the pERG amplitude from the peak of P50 to trough of N95 showed a significant decrease in the Sod3 knockout mice compared to controls (middle; $p = 0.0054$), while the N95 latency was lower but not significant between the two groups (bottom; $p = 0.22$). N = 7 mice per group. Error bars = standard deviation. *, $p < 0.01$.

PERG responses in DVR patients without late clinical pathology (no epiretinal membranes, cataracts, or other severe clinical presentations) displayed diminished inner retina function despite normal outer retina (photoreceptor) function (red) compared to a control patient (black; Fig. 6B). At later stages of DVR, despite control of retinal neovascularization following laser photocoagulation of the peripheral retina, patients develop progressive fibrosis along the vitreoretinal interface (Fig. 6C). The normally clear vitreous cortex becomes opaque due to fibrotic membranes exerting traction on the retinal surface, as can be confirmed by infrared imaging (Fig. 6D). IHC of the vitreoretinal membrane from a DVR patient showed vitreoretinal adhesion, tractional retinal detachment, and an epiretinal membrane (Fig. 6E). Together, these indicate a dysfunction at the vitreoretinal interface leading to visual impairment in patients presenting with DVR. Disruption of oxidative stress management mechanisms at this interface could account in part for defects in the inner retina, suggesting a role for SOD3 in DVR.

2.8. SOD3 activity in diabetic vitreoretinopathy

IHC of epiretinal membranes from a human DVR patient showed SOD3 expression (green), as well as decorin (red; Fig. 7A), but they were not co-localized. Since SOD3 was present in the fibrous epiretinal membranes near the inner retina of DVR patients, it's possible that SOD3 dysregulation at the vitreous base may lead to changes in oxidative stress at the vitreoretinal interface. We measured changes in oxidative stress in human DVR patients and found that reducible nitrate concentrations were significantly increased ($p = 0.036$), and on average there was more than a two-fold increase in DVR vitreous samples compared to control samples (Fig. 7B). We have previously published a mouse model for proliferative diabetic retinopathy (PDR), where the von Hippel Lindau tumor suppressor protein (VHL) was knocked out within the photoreceptor cells [25]. IHC for 3-nitrotyrosine in the vitreous of this mouse model for PDR showed a severe increase in oxidative stress in the vitreous compared to both wild-type and *Sod3* knockout mice (Fig. 7C). Elevation of intraocular reactive oxygen species (ROS) in the vitreous is implicated in the pathogenesis of DVR, as well as other vitreoretinopathies, but the molecular mechanisms are not known. We have shown that SOD3 is differentially localized to the vitreous base through heparin interactions and acts to prevent oxidative damage at the vitreoretinal interface. Therefore, dysregulation of SOD3 may be critical in the pathophysiology of DVR.

3. Discussion

The goal of this investigation was to better understand the role the vitreous might play in the regulation of oxidative stress that affects the neural retina. We sought differentially expressed molecules from our

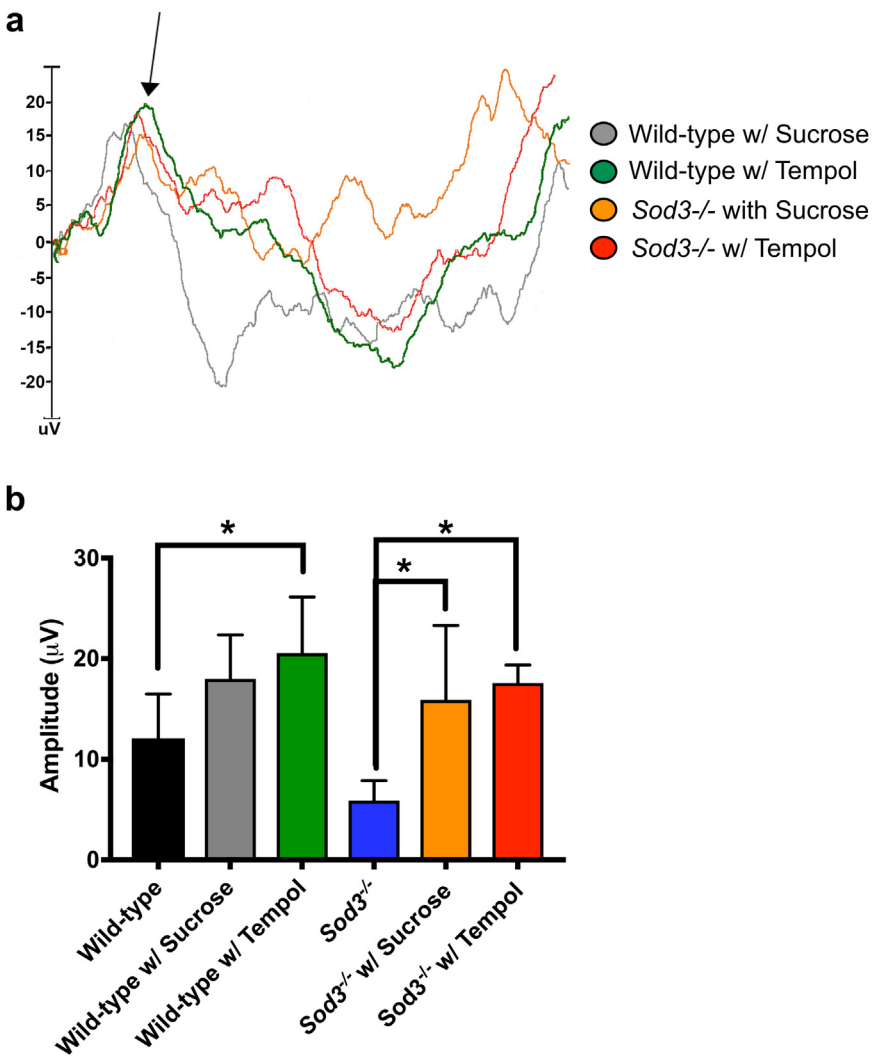

Fig. 5. Sod3 inner retinal dysfunction is rescued after treatment with sucrose and a potent antioxidant. (A) Representative traces from the experimental PERGs for mice with sucrose delivery via the drinking water (*Sod3*$^{-/-}$ mouse, orange; wild-type mouse, gray) and with the addition of tempol, a potent antioxidant, to the drinking water (*Sod3*$^{-/-}$ mouse, red; wild-type mouse, green). PERG amplitude is marked by an arrow. (B) Quantification of the PERG amplitudes showed a significant restoration in amplitude in the *Sod3* knockout mice after both sucrose ($p = 0.0141$; orange) and tempol delivery ($p = 0.0151$; red) in comparison to untreated *Sod3* knockout mice (blue). There was also a significant restoration of PERG amplitude in wild-type mice treated with Tempol and sucrose (green) in comparison to untreated wild-type mice ($p = 0.0353$; black). There was no significant difference between untreated wild-type mice (black) and wild-type mice with sucrose treatment ($p = 0.3698$; gray). There was also no significant difference between mice treated with sucrose alone compared to mice treated with Tempol and sucrose ($p = 0.9566$ for wild-type mice and $p = 0.9961$ for *Sod3*$^{-/-}$ mice). $N \geq 3$ mice per group. Error bars = standard deviation. *, $p < 0.05$.

proteomics data and studied their role in vitreoretinal disease. This study utilized a novel method to dissect human vitreous from the cortex, core, and base. In fresh human donor eyes, IHC of superoxide dismutase-3 (SOD3) revealed a remarkable pattern of expression: SOD3 showed a punctate pattern following a “looping” found at the vitreous base and cortex (Fig. 2B, C). This “looping pattern” has not been described previously, and its composition is not known.

In non-ocular tissues, SOD3 is sequestered to heparin and collagen I [26,27]. Binding to these extracellular substances represents a way for SOD3 to be concentrated where its activity is required. The eye is an area of high oxidative stress due to UV radiation, high metabolic activity, and high oxygen tension [28], and it would be likely for SOD3 to play a key role in the regulation of oxidative stress within the eye. Since sulfate proteoglycans and several collagens are primary constituents of the human vitreous base and cortex, these are likely interaction candidates for SOD3 within the vitreous. We demonstrated that SOD3 binds with heparin in the vitreous base, but not the other tested proteoglycans from the vitreous (i.e. decorin and aggrecan). Sequestration of SOD3 in areas of oxidative damage is crucial to prevent the superoxide radical from reacting promiscuously with neighboring structures. The pattern of localization for SOD3 suggests the presence of a specific interaction(s) to keep SOD3 adjacent to the inner retina, ciliary body, and lens where it can protect these tissues from oxidative damage. This may be particularly important to the inner retina, the site of the neuronal cell signaling complexes, as well as the ciliary body, which produces the aqueous humor that provides oxygenation and nutrients to the lens and cornea.

Our study confirmed Sod3 to be present in the vitreous base and cortex of mice, similar to humans. *Sod3* knockout mice were examined for potential ocular phenotypes, as they had not been previously characterized for eye abnormalities. Our results demonstrate that nitrates were variable but not altered between *Sod3*$^{-/-}$ mice and control mice, but that 3-nitrotyrosine was present in both the vitreous and the retinal ganglion cells (RGCs), with the highest levels at the vitreoretinal interface. Along with increased oxidative stress at the vitreoretinal interface, *Sod3*$^{-/-}$ mice had a loss of PERG function in comparison with controls, which was rescued following treatment with sucrose and an antioxidant, suggesting that the loss of Sod3 in the vitreous causes changes in the oxidative stress response of the inner neural retina that leads to vision defects.

The rescue effect visible after sucrose delivery is likely due to the high metabolic activity of the photoreceptor cells. It has been shown in mice that rod photoreceptor cells rely on glycolysis for their outer segment biogenesis [29]. Additionally, previous studies have shown that glucose is able to reduce ROS in cultured rat retinal cells by acting on both the glycolytic and pentose phosphate pathways [30], and that enhancing glycolysis in the photoreceptor cells and releasing retained glucose from the RPE to starving photoreceptors provide short-term rescue effects to models of retinitis pigmentosa [31]. Even a high carbohydrate diet, raising blood glucose levels, improved retinal function in disease systems, but was unable to restore the synaptic contacts at the retinal ganglion cell layer [32]. SOD3 has been shown to increase

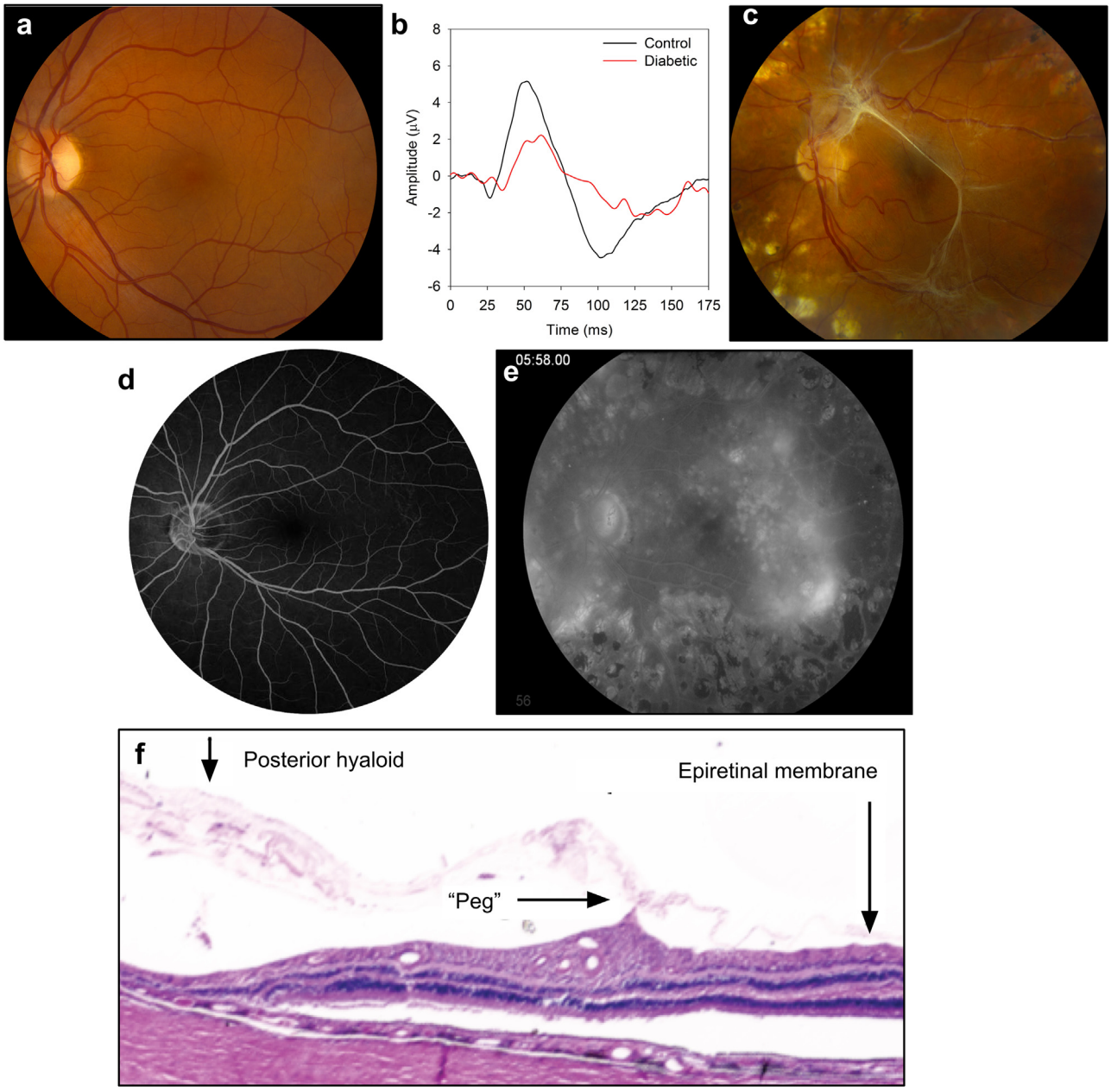

Fig. 6. Clinical pathology of human diabetic vitreoretinopathy. (A) Normal human fundus image. (B) pERG traces displaying a reduction in visual response in human patients with early-stage diabetic vitreoretinopathy (DVR; red) compared to normal human patients (black). (C) Fundus image of a patient with later-stage DVR. (D) Infrared image from a patient with DVR displaying inflammation and hemorrhaging within the eye. (E) IHC of the posterior hyaloid and vitreoretinal membrane from a patient with DVR showing the presence of an epiretinal membrane, vitreoretinal adhesion and tractional retinal detachment.

glucose metabolism [33] as an additional mechanism of reducing ROS levels. We have recently observed, using gene ontology, that antioxidant activity was highly expressed in the juxta-macular and peripheral retina, and that metabolic pathways were differentially expressed in various retinal regions (foveomacular, juxta-macular and peripheral retinal regions) in the human eye [34]. Therefore, the addition of sucrose and its effect on metabolic regulation in the inner retina may be masking the increased oxidative stress caused by a loss of Sod3. In human patients, it may be possible to alleviate retinal disorders related to SOD3 dysregulation by direct injection of either glucose or a Tempol compound into the intravitreal space of the eye.

Mouse models of diabetes have implicated a role of both Sod1 and Sod3 in increased levels of superoxide anions and vascular tissue damage, phenotypes also found in diabetic humans. In KK/Ta-Akita diabetic mice, for example, levels of Sod1 and Sod3 are below normal, corresponding to elevated levels of superoxide production and decreased glomeruli filtering function [35]. Increased infiltration of inflammatory cells as well as increased fibrosis have been demonstrated in lung and heart tissues of the *Sod3*$^{-/-}$ mouse [36,37]. In our murine model of proliferative diabetic retinopathy [25], we found increased 3-nitrotyrosine within the vitreous, indicative of high oxidative stress. The *Sod3*$^{-/-}$ mice show that the absence or dysregulation of Sod3 results in increased oxidative stress and tissue damage, a phenotype not previously studied with this murine model system, and this phenotype shows clinical similarities to that seen in DVR patients and patients of other vitreoretinopathies.

Additionally, many studies have linked increased oxidative stress to development of diabetes related complications, including DVR [38]. Elevated glucose levels cause the release of ROS which is considered to be a causal link between the metabolic abnormalities in diabetic

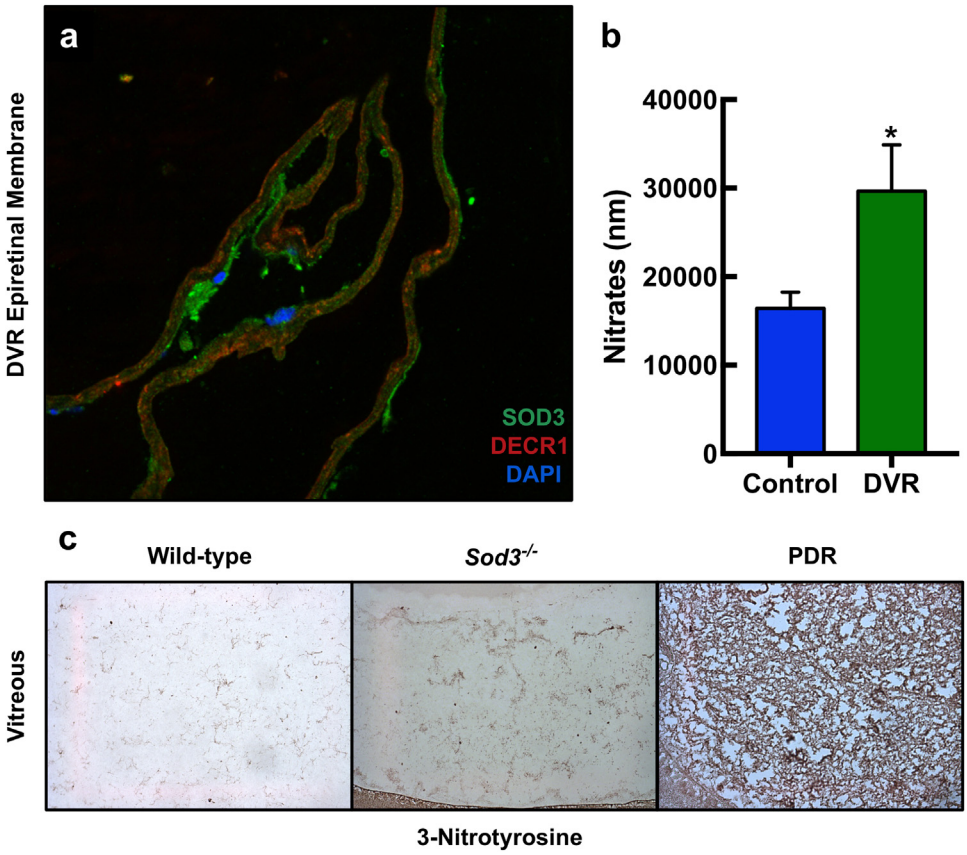

Fig. 7. A role for SOD3 in the regulation of oxidative stress in diabetic vitreoretinopathy. (A) IHC in an epiretinal membrane from a human with DVR showed SOD3 (green) and decorin (red), but no co-localization. Cell nuclei are stained with DAPI (blue). (B) Nitrates were found to be significantly increased in human DVR patients compared to controls ($p = 0.036$). *, $p < 0.05$. Error bars = standard deviation. N = 9 controls, 10 DVR patients. (C) IHC showed increased levels of 3-nitrotyrosine in the Sod3 knockout mice (middle), and a severe increase in 3-nitrotyrosine in a mouse model for proliferative diabetic retinopathy (right), compared to wild-type controls (left).

patients and the development of complications. We examined SOD3 in human DVR patients using biopsies of the vitreous and epiretinal membranes. We found that SOD3 is present in epiretinal membranes from the DVR patient vitreous samples. Nitrates were also significantly increased in DVR patients compared to controls, providing further evidence for increased oxidative stress in the eyes of diabetic subjects. Our results suggest that patients with DVR have increased levels of oxidative stress at the vitreoretinal interface, possibly due to the dysregulation of SOD3 in the vitreous base.

Based on our findings, SOD3 compartmentalizes to the vitreous base and cortex, regulates oxidative stress at the vitreoretinal interface, and influences electrophysiology at the inner neural retina. Understanding how SOD3 is localized to specific vitreous substructures may provide insight into the molecular mechanisms regulating intraocular oxidative stress in DVR. Furthermore, since intraocular oxidative stress is associated with the pathogenesis of age-related macular degeneration [39] and glaucoma [40], these experiments have implications for other blinding eye diseases. Overall, regulation of SOD3 at the vitreous base and cortex may represent a future therapeutic target for vitreoretinal diseases. Future studies are needed to further elucidate the binding activity of SOD3 at the vitreoretinal interface and the mechanism by which it protects the inner retina.

4. Materials and methods

The study protocol was approved by the Institutional Review Board for Human Subjects Research (IRB) at the University of Iowa and Stanford University, was HIPAA compliant, and adhered to the tenets of the Declaration of Helsinki. All subjects underwent informed consent for study participation. All experiments were performed in accordance with the ARVO Statement for the Use of Animals in Ophthalmic and Visual Research and were all approved by the Animal Care and Use Committee at the University of Iowa and Stanford University.

4.1. Human vitreous biopsies

A 23 gauge vitreous cutter (Alcon Laboratories Inc, Fort Worth, TX) was inserted and the cutter was activated for 30 s. A 250 − 500 mL vitreous was then manually aspirated into a second syringe. Following sampling the vitreous, a core vitrectomy proceeded as normal. Vitreous samples were immediately centrifuged in the operating room at 15,000 *g* for 5 min at room temperature to remove particulate matter. All samples were then stored at − 80 °C.

4.2. Human vitreous dissection

Human donor eyes were dissected within four hours or less from death. The cornea was cut circumferentially around the limbus and removed. The iris was then removed by cutting circumferentially at near the ciliary body using curved Westcott scissors. Next, the vitreous core was aspirated using a 23 gauge needle until completely removed. Aspirating the vitreous core allows the anterior hyaloid to be easily visualized as a transparent ring within the anterior opening where the cornea was removed. This tissue was very carefully grasped using 0.12 colibri forceps and pulled away from the ciliary body. Small vannas scissors were used to cut the anterior hyaloid away from the ciliary body and sclera. After all of the hyaloid was collected, the eye cup was flowered into four quadrants and the ciliary body was removed from each quadrant. Using 0.22 mm forceps, the vitreous base was pulled up from the region spanning the pars plana, ora serrata, and 3 mm posterior to the ora serrata, while Westcott scissors were used to cut the vitreous base away from the other tissues. Vitreous base was collected from all four quadrants and then the ora serrata, including 3 mm posterior, was cut and removed from the quadrants as well. The posterior cortex was lifted away from the retina using 0.12 colibri forceps and cut using Westcott scissors. All samples were put into a 1.5 mL tube and frozen in liquid nitrogen immediately after collection.

4.3. Human posterior hyaloid excision

Surgical intervention with vitrectomy, posterior hyaloid dissection and epiretinal membrane peeling was performed on a 66-year-old male with type 2 diabetes mellitus controlled on oral hypoglycemic agents and a history of bilateral proliferative diabetic retinopathy previously treated with extensive panretinal photocoagulation. He had clinically significant macular edema OS and vitreomacular traction with a vision of 20/50 OS, after undergoing extensive focal laser treatment. The patient had diffuse leakage from areas of chronic neovascularization along the inferotemporal arcade, which corresponded to areas of significant vitreoretinal traction as noted on OCT. Intravitreal bevicizumab was provided in an attempt to reduce the edema, which was ineffective.

4.4. Imaging

Fundus SW-AF and SD-OCT images were obtained in all patients after dilation using Spectralis HRA + OCT device (Heidelberg Engineering, Heidelberg, Germany). SW-AF images were acquired using a 30-degree field of view with 1536 × 1536 pixel resolution. SW-AF imaging utilized a 521 nm barrier filter and 486 nm wavelength stimulus. The external horizontal and vertical ring diameter of SW-AF imaging was measured manually using Spectralis software (Heidelberg Eye explorer, software version 1.9.10, Heidelberg Engineering). SD-OCT was obtained with an 870 nm light source and automatic real-time registration of the fundus infrared reflectance image. Horizontal scans (high resolution mode, 9 mm, ART, average of a minimum of 50 images) through the fovea provided a view of the EZ-line and was measured manually using Spectralis software. IR fundus imaging was obtained with the Spectralis scanning laser confocal ophthalmoscope (Heidelberg Engineering). IR imaging was obtained at 790 nm absorption and 830 nm emission using a 55° lens.

4.5. *Sod3*$^{-/-}$ mice

Sod3 knockout mice were generously provided by the Dr. Tim D. Oury laboratory (Department of Pathology, University of Pittsburgh Medical Center, Pittsburgh, PA). *Sod3*$^{-/-}$ mice were back-crossed into the C57BL/6 genetic background and C57BL/6J mice (the Jackson Laboratory, Bar Harbor, ME) were purchased and used as controls.

4.6. Mouse vitreous biopsies

The vitreous from 8 mouse eyes were eviscerated as described previously [19,41]. Briefly, scleral tissue posterior to the limbus was grasped with a 0.22 forcep and a microsurgical blade was used to make a linear incision in the cornea from limbus to limbus. A fine curved needle holder was inserted behind the lens and then pulled forward, eviscerating both the lens and the vitreous. The lens-vitreous tissue was centrifuged with 20 μL of protease inhibitor cocktail (Roche) dissolved in PBS. The fine curved needle holder was placed as far posterior to the globe as possible and the retina was eviscerated through the corneal incision. Some vitreous also came with the retina. The retina-vitreous tissue was also filtered. The filtered centrifuge tube was spun at 14,000 *g* for 12 min and the eluent (vitreous) was collected.

4.7. Protein analysis

Total protein was measured using a NanoDrop 2000 spectrophotometer (NanoDrop, Wilmington, DE). Protein quantity was determined via absorbance at 280 nm [42].

4.8. Nitrate measurement

Levels of NO were measured in the gas phase using a Sievers NOA 280i chemiluminescence analyzer (Sievers NOA, Boulder, CO). Samples were injected into a nitrogen purge vessel containing a 1% solution of sodium iodide in glacial acetic acid to liberate gaseous NO from dissolved NO and nitrite. The sample gas was then exposed to ozone in the reaction vessel to form activated nitrogen dioxide (NO_2*), which was detected by a red-sensitive photomultiplier tube and the output recorded using an integrating pen recorder. For each sample, the area under the curve was converted to pmol NO using a calibration curve constructed following the analysis of a series of sodium nitrite standards.

4.9. 3-Nitrotyrosine immunohistochemistry

Oxidative damage was localized in paraffin sections of mouse ocular tissues by staining with an anti-nitrotyrosine antibody (StressMarq Biosciences Inc.; Victoria, British Columbia, Canada) as previously described [43].

4.10. SOD activity assay

Human post mortem vitreous base was dissected to obtain 50 mg pieces. The samples were incubated either with 250 μL of 50 mM D-glucose (n = 10) or phosphate buffer alone (n = 5) at room temperature for 45 min. Following incubation, samples were spun at 1000 *g* for 5 min. The supernatant was collected, being careful to avoid the vitreous base matrix at the bottom of the tube and applied to the Superoxide Dismutase Activity Colorimetric Assay Kit (Abcam product #ab65354). Activity is indicative of SOD3 released from the vitreous base into the supernatant solution. Xanthine Oxidase was measured using the Xanthine Oxidase Activity Assay Kit (Abcam; ab102522).

4.11. Dot blot array

We created a protein array of potential SOD3 binding partners by dot blotting specific proteins (200 ng) in quadruplicate onto nitrocellulose membranes (BioRad, #162-0112) as previously described [44]. Selected proteins include new vitreous collagens identified in our vitreous proteome library, as well as previously known vitreous collagens [45,46]. Following crosslinking of the proteins, blots were incubated with 1 μg/mL of a human GST-SOD3 fusion protein (Protein Tech, #ag5556), and then an HRP conjugated anti-GST antibody at 1:1000 (GE Healthcare, #RPN1236). Protein-protein interactions were visualized and compared simultaneously with chemiluminescence detection [47]. Recombinant SOD3 missing the heparin-binding domain (ECSODΔHBD) or mutated with R213G were expressed in MIA PaCa-2 cells by a replication defective adenoviral vector; available through the UI Radiation and Free Radical Research Core [44,48]. Mutant fusion proteins were incubated with protein array blots, and interactions were detected with an HRP conjugated anti-GST antibody as described above.

4.12. Human immunohistochemistry

Human donor tissue was collected from postmortem eyes. Tissue was embedded in optimal cutting temperature (OCT) medium and frozen. Sections of ciliary body (including vitreous base) and sections of macular retina and choroid (some including posterior hyaloid) were collected at a thickness of 7 μm using a Microm cryostat equipped with Cryo Jane adhesive tape onto Superfrost Plus slides (Fisher). Sections were blocked with 0.1% bovine serum albumin in PBS for 15 min. Following the block, sections were incubated with rabbit anti-human collagen IV and rabbit anti-human SOD3 (Abcam) antibodies diluted in PBS for 1 h. Antibody incubation was followed by 3 × 5 min rinses in PBS. Sections were incubated with goat anti-rabbit AlexaFluor 488, AlexaFluor 594 and DAPI (Invitrogen, Eugene, OR).

4.13. Intra-Ocular Pressure Recordings

Mice were anesthetized with an IP injection of 100 mg/kg ketamine hydrochloride and 5 mg/kg xylazine. Using sterile probes, a tonometer designed for the mouse eye was pressed against the cornea and used to record a series of 5 measurements over approximately 10 s.

4.14. Pattern Electroretinogram (PERG)

Pattern-evoked electroretinography (PERG) was used to objectively measure the function of RGCs by recording the amplitude of the PERG waveform following TBI. Mice were anesthetized with a combination of ketamine (0.03 mg/g, IP) and xylazine (0.005 mg/g, IP), and then placed on a heated recording table to maintain body temperature. Neutral position PERG responses were evoked using alternating, reversing, and black and white vertical stimuli delivered on a monitor (Jorvec, Miami, FL) and recorded using a nose electrode. A reference needle electrode was placed at the base of the head, and a ground electrode was placed at the base of the tail to complete the circuit. Each animal was placed at the same fixed position in front of the monitor to prevent recording variability due to animal placement. Stimuli (188 radius visual angle subtended on full field pattern, 2 reversals per second, 372 averaged signals with cut off filter frequencies of 1–30 Hz, 98% contrast, 80 cd/m^2 average monitor illumination intensity) were delivered under mesopic conditions without dark adaptation to exclude the possible effect of direct photoreceptor-derived evoked responses. A diffuser placed over the pattern on the monitor also did not elicit a measurable evoked potential, further ensuring that the electrical responses were elicited from the RGCs. The PERG response was evaluated by measuring the amplitude (peak to trough) of the waveform. Human PERG data was recorded according to ISCEV standards. The black trace represents the mean response of 15 visually-normal subjects, and the red trace is from a type 2 diabetic patient (59 years old, 20/25 VA, moderate-severe NPDR, no history of treatment). Rescue experiments were performed as described previously [49]. Briefly, Tempol (Sigma-Aldrich Co.) was dissolved in ethanol vehicle and administered at 25 nM in the drinking water. Sucrose (4 g/100 mL) was supplemented in the water bottles to offset the taste of the antioxidant. Mice were treated at weaning (post-natal day 21) until the end of the experiment.

4.15. Statistical analyses

Differences in experimental groups were determined by the Student's *t*-test as appropriate, or by one-way ANOVA followed by Tukey's post-hoc multiple comparison's test. p values < 0.05 were considered significant.

Acknowledgements

Author Contributions: Dr. Mahajan had full access to all the data in the study and takes responsibility for the integrity of the data and the accuracy of the data analysis. Study concept and design: VBM. Acquisition of data: KJW, BAW, MLT, GV, FED, GRB, JM, AO, MMH, VBM. Analysis and interpretation of data: KJW, GV, SHT, AGB, VBM. Drafting of the manuscript: KJW, MRC, GV, SHT, AGB, VBM. Critical revision of the manuscript for important intellectual content: KJW, SHT, AGB, VBM. Statistical analysis: KJW, GV, VBM. Obtained funding: VBM. We are grateful to the Oury laboratory for their generous donation of the *Sod3* knockout mice.

Conflict of interest disclosures

None reported.

Funding/support

VBM and AGB are supported by NIH grants [R01EY026682, R01EY024665, R01EY025225, R01EY024698, R21AG050437 and P30EY026877], The Doris Duke Charitable Foundation Grant #2013103, and Research to Prevent Blindness (RPB), New York, NY. GV is supported by NIH grants [F30EYE027986 and T32GM007337]. The Barbara & Donald Jonas Laboratory of Regenerative Medicine and Bernard & Shirlee Brown Glaucoma Laboratory are supported by the National Institute of Health [5P30EY019007, R01EY018213, R01EY024698, R21AG050437], National Cancer Institute Core [5P30CA013696], the Research to Prevent Blindness (RPB) Physician-Scientist Award, unrestricted funds from RPB, New York, NY, USA. JM is supported by NIH grants R01EY026004 and P30EY001792 and a Research to Prevent Blindness (RPB) Special Scholar award. SHT is a member of the RD-CURE Consortium and is supported by the Tistou and Charlotte Kerstan Foundation, the Schneeweiss Stem Cell Fund, New York State [C029572], the Joel Hoffman Fund, the Professor Gertrude Rothschild Stem Cell Foundation, and the Gebroe Family Foundation.

Role of the sponsor

The funding organizations had no role in design and conduct of the study; collection, management, analysis, and interpretation of the data; preparation, review, or approval of the manuscript; and decision to submit the manuscript for publication.

Appendix A. Supporting information

Supplementary data associated with this article can be found in the online version at http://dx.doi.org/10.1016/j.freeradbiomed.2018.06.024.

References

[1] M. Che, R. Wang, X. Li, H.Y. Wang, X.F. Zheng, Expanding roles of superoxide dismutases in cell regulation and cancer, Drug Discov. Today 21 (2016) 143–149.
[2] T. Fukai, M. Ushio-Fukai, Superoxide dismutases: role in redox signaling, vascular function, and diseases, Antioxid. Redox Signal. 15 (2011) 1583–1606.
[3] D. Sim, M. Fruttiger, Keeping blood vessels out of sight, Elife 2 (2013) e00948.
[4] Z. Géhl, E. Bakondi, M.D. Resch, C. Hegedűs, K. Kovács, P. Lakatos, A. Szabó, Z. Nagy, L. Virág, Diabetes-induced oxidative stress in the vitreous humor, Redox Biol. 9 (2016) 100–103.
[5] M. Kuroki, E.E. Voest, S. Amano, L.V. Beerepoot, S. Takashima, M. Tolentino, R.Y. Kim, R.M. Rohan, K.A. Colby, K.T. Yeo, et al., Reactive oxygen intermediates increase vascular endothelial growth factor expression in vitro and in vivo, J. Clin. Investig. 98 (1996) 1667–1675.
[6] A. Dong, B. Xie, J. Shen, T. Yoshida, K. Yokoi, S.F. Hackett, P.A. Campochiaro, Oxidative stress promotes ocular neovascularization, J. Cell Physiol. 219 (2009) 544–552.
[7] S. Kubota, T. Kurihara, H. Mochimaru, S. Satofuka, K. Noda, Y. Ozawa, Y. Oike, S. Ishida, K. Tsubota, Prevention of ocular inflammation in endotoxin-induced uveitis with resveratrol by inhibiting oxidative damage and nuclear factor-kappaB activation, Investig. Ophthalmol. Vis. Sci. 50 (2009) 3512–3519.
[8] P. Tokarz, K. Kaarniranta, J. Blasiak, Role of antioxidant enzymes and small molecular weight antioxidants in the pathogenesis of age-related macular degeneration (AMD), Biogerontology 14 (2013) 461–482.
[9] J.Y. Jang, H. Cho, H.Y. Park, H. Rhim, S. Kang, ALS-linked mutant SOD1 proteins promote Abeta aggregates in ALS through direct interaction with Abeta, Biochem. Biophys. Res. Commun. 493 (2017) 697–707.
[10] J.R. Peng, et al., Elevated levels of plasma superoxide dismutases 1 and 2 in patients with coronary artery disease, BioMed. Res. Int. (2016) 3708905.
[11] E. Srinivasan, R. Rajasekaran, Exploring the cause of aggregation and reduced Zn binding affinity by G85R mutation in SOD1 rendering amyotrophic lateral sclerosis, Proteins 85 (2017) 1276–1286.
[12] C. Tian, T. Liu, S. Fang, X. Du, C. Jia, Association of C47T polymorphism in SOD2 gene with coronary artery disease: a case-control study and a meta-analysis, Mol. Biol. Rep. 39 (2012) 5269–5276.
[13] S.V. Petersen, D.A. Olsen, J.M. Kenney, T.D. Oury, Z. Valnickova, I.B. Thogersen, J.D. Crapo, J.J. Enghild, The high concentration of Arg213– > Gly extracellular superoxide dismutase (EC-SOD) in plasma is caused by a reduction of both heparin and collagen affinities, Biochem. J. 385 (2005) 427–432.
[14] C.J. Kobvlecki, S. Afzal, B.G. Nordestgaard, Genetically low antioxidant protection and risk of cardiovascular disease and heart failure in diabetic subjects, EBioMedicine 2 (2015) 2010–2015.

[15] J.M. Skeie, C.N. Roybal, V.B. Mahajan, Proteomic insight into the molecular function of the vitreous, PLoS One 10 (2015) e0127567.
[16] T. Cabral, et al., Dissection of human retina and RPE-choroid for proteomic analysis, J. Vis. Exp. (2017), http://dx.doi.org/10.3791/56203.
[17] L. Paemka, V.B. Mahajan, S.N. Ehaideb, J.M. Skeie, M.C. Tan, S. Wu, A.J. Cox, L.P. Sowers, J. Gecz, L. Jolly, et al., Seizures are regulated by ubiquitin-specific peptidase 9 X-linked (USP9X), a de-ubiquitinase, PLoS Genet. 11 (2015) e1005022.
[18] L. Paemka, V.B. Mahajan, J.M. Skeie, L.P. Sowers, S.N. Ehaideb, P. Gonzalez-Alegre, T. Sasaoka, H. Tao, A. Miyagi, N. Ueno, et al., PRICKLE1 interaction with SYNAPSIN I reveals a role in autism spectrum disorders, PLoS One 8 (2013) e80737.
[19] J.M. Skeie, V.B. Mahajan, Proteomic interactions in the mouse vitreous-retina complex, PLoS One 8 (2013) e82140.
[20] C.C.F. Bernardy, A.C. Zarpelon, F.A. Pinho-Ribeiro, C. Calixto-Campos, T.T. Carvalho, V. Fattori, S.M. Borghi, R. Casagrande, W.A. Verri, Tempol, a superoxide dismutase mimetic agent, inhibits superoxide anion-induced inflammatory pain in mice, Biomed. Res. Int. 2017 (2017) 9584819.
[21] Q.S. Zhang, L. Eaton, E.R. Snyder, S. Houghtaling, J.B. Mitchell, M. Finegold, C. Van Waes, M. Grompe, Tempol protects against oxidative damage and delays epithelial tumor onset in Fanconi anemia mice, Cancer Res. 68 (2008) 1601–1608.
[22] R. Schubert, L. Erker, C. Barlow, H. Yakushiii, D. Larson, A. Russo, J.B. Mitchell, A. Wynshaw-Boris, Cancer chemoprevention by the antioxidant tempol in Atm-deficient mice, Hum. Mol. Genet. 13 (2004) 1793–1802.
[23] P.K. Chatterjee, S. Cuzzocrea, P.A. Brown, K. Zacharowski, K.N. Stewart, H. Mota-Filipe, C. Thiemermann, Tempol, a membrane-permeable radical scavenger, reduces oxidative stress-mediated renal dysfunction and injury in the rat, Kidney Int. 58 (2000) 658–673.
[24] C. Li, X. Miao, F. Li, S. Wang, Q. Liu, Y. Wang, J. Sun, Oxidative stress-related mechanisms and antioxidant therapy in diabetic retinopathy, Oxid. Med. Cell Longev. 2017 (2017) 9702820.
[25] K.J. Wert, V.B. Mahajan, L. Zhang, Y. Yan, Y. Li, J. Tosi, C.W. Hsu, T. Nagasaki, K.M. Janisch, M.B. Grant, M. Mahajan, A.G. Bassuk, S.H. Tsang, Neuroretinal hypoxic signaling in a new preclinical murine model for proliferative diabetic retinopathy, Signal Transduct. Target Ther. 1 (2016) (pii: 16005).
[26] S.V. Petersen, J.J. Enghild, Extracellular superoxide dismutase: structural and functional considerations of a protein shaped by two different disulfide bridge patterns, Biomed. Pharmacother. 59 (2005) 175–182.
[27] S.V. Antonyuk, R.W. Strange, S.L. Marklund, S.S. Hasnain, The structure of human extracellular copper-zinc superoxide dismutase at 1.7 A resolution: insights into heparin and collagen binding, J. Mol. Biol. 388 (2009) 310–326.
[28] Y. Chen, G. Mehta, V. Vasiliou, Antioxidant Defenses in the ocular surface, Ocul. Surf. 7 (2009) 176–185.
[29] Y. Chinchore, T. Begaj, D. Wu, E. Drokhlyansky, C.L. Cepko, Glycolytic reliance promotes anabolism in photoreceptors, eLife 6 (2017) e25946.
[30] G. Han, J.P. Wood, G. Chidlow, T. Mammone, R.J. Casson, Mechanisms of neuroprotection by glucose in rat retinal cell cultures subjected to respiratory inhibition, Investig. Ophthalmol. Vis. Sci. 54 (2013) 7567–7577.
[31] H.J. Kaplan, W. Wang, D.C. Dean, Restoration of cone photoreceptor function in retinitis pigmentosa, Transl. Vis. Sci. Technol. 6 (2017) 5.
[32] Y. Umino, N. Cuenca, D. Everhart, L. Fernandez-Sanchez, R.B. Barlow, E. Solessio, Partial rescue of retinal function in chronically hypoglycemic mice, Investig. Ophthalmol. Vis. Sci. 53 (2012) 915–923.
[33] J.P. Laurila, M.D. Castellone, A. Curcio, L.E. Laatikainen, M. Haaparanta-Solin, T.J. Gronroos, P. Marjamaki, S. Martikainen, M. Santoro, M.O. Laukkanen, Extracellular superoxide dismutase is a growth regulatory mediator of tissue injury recovery, Mol. Ther. 17 (2009) 448–454.
[34] G. Velez, D.A. Machlab, P.H. Tang, Y. Sun, S.H. Tsang, A.G. Bassuk, V.B. Mahajan, Proteomic analysis of the human retina reveals region-specific susceptibilities to metabolic- and oxidative stress-related diseases, PLoS One 13 (2018) e0193250.
[35] H. Fujita, H. Fujishima, S. Chida, K. Takahashi, Z. Qi, Y. Kanetsuna, M.D. Breyer, R.C. Harris, Y. Yamada, T. Takahashi, Reduction of renal superoxide dismutase in progressive diabetic nephropathy, J. Am. Soc. Nephrol. 20 (2009) 1303–1313.
[36] C.L. Fattman, R.J. Tan, J.M. Tobolewski, T.D. Oury, Increased sensitivity to asbestos-induced lung injury in mice lacking extracellular superoxide dismutase, Free Radic. Biol. Med. 40 (2006) 601–607.
[37] C.R. Kliment, H.B. Suliman, J.M. Tobolewski, C.M. Reynolds, B.J. Day, X. Zhu, C.F. McTiernan, K.R. McGaffin, C.A. Piantadosi, T.D. Oury, Extracellular superoxide dismutase regulates cardiac function and fibrosis, J. Mol. Cell Cardiol. 47 (2009) 730–742.
[38] R.A. Kowluru, P.S. Chan, Oxidative stress and diabetic retinopathy, Exp. Diabetes Res. 2007 (2007) 43603.
[39] S. Khandhadia, A. Lotery, Oxidation and age-related macular degeneration: insights from molecular biology, Expert Rev. Mol. Med. 12 (2010) e34.
[40] D.M. Kumar, N. Agarwal, Oxidative stress in glaucoma: a burden of evidence, J. Glaucoma 16 (2007) 334–343.
[41] J.M. Skeie, S.H. Tsang, V.B. Mahajan, Evisceration of mouse vitreous and retina for proteomic analyses. J. Vis. Exp. pii: 2795, 2011.
[42] C.M. Stoscheck, Quantitation of protein, Methods Enzymol. 182 (1990) 50–68.
[43] R. Tao, M.C. Coleman, J.D. Pennington, O. Ozden, S.H. Park, H. Jiang, H.S. Kim, C.R. Flynn, S. Hill, W. Hayes McDonald, et al., Sirt3-mediated deacetylation of evolutionarily conserved lysine 122 regulates MnSOD activity in response to stress, Mol. Cell 40 (2010) 893–904.
[44] Y. Chu, A. Alwahdani, S. Iida, D.D. Lund, F.M. Faraci, D.D. Heistad, Vascular effects of the human extracellular superoxide dismutase R213G variant, Circulation 112 (2005) 1047–1053.
[45] J. Sebag, Molecular biology of pharmacologic vitreolysis, Trans. Am. Ophthalmol. Soc. 103 (2005) 473–494.
[46] P.N. Bishop, Structural macromolecules and supramolecular organisation of the vitreous gel, Prog. Retin Eye Res. 19 (2000) 323–344.
[47] J.M. Skeie, V.B. Mahajan, Dissection of human vitreous body elements for proteomic analysis. J. Vis. Exp. pii: 2455, 2011.
[48] M.L. Teoh, M.P. Fitzgerald, L.W. Oberley, F.E. Domann, Overexpression of extracellular superoxide dismutase attenuates heparanase expression and inhibits breast carcinoma cell growth and invasion, Cancer Res. 69 (2009) 6355–6363.
[49] A.J. Case, J.L. McGill, L.T. Tygrett, T. Shirasawa, D.R. Spitz, T.J. Waldschmidt, K.L. Legge, F.E. Domann, Elevated mitochondrial superoxide dismutase disrupts normal T cell development, impairing adaptive immune responses to an influenza challenge, Free Radic. Biol. Med. 50 (2011) 448–458.